ECI Symposium Series, Volume RP5: Proceedings of 7th International Conference on Heat Exchanger Fouling and Cleaning - Challenges and Opportunities, Editors Hans Müller-Steinhagen, M. Reza Malayeri, and A. Paul Watkinson, Engineering Conferences International, Tomar, Portugal, July 1 - 6, 2007

INFLUENCE OF DIFFERENT SURFACE MATERIALS ON NUCLEATION AND CRYSTAL GROWTH IN HEAT EXCHANGERS

T. Geddert[1], S. Kipp[2],W. Augustin[3] and S. Scholl[4]
[1, 3, 4] Technical University of Braunschweig, Institute for Chemical and Thermal Process Engineering, Langer Kamp 7, 38106 Braunschweig, Germany; t.geddert@tu-bs.de[1], w.augustin@tu-bs.de[3], s.scholl@tu-bs.de[4]
[2] Technical University of Braunschweig, Institute for Physical and Theoretical Chemistry, Hans-Sommer-Strasse 10, 38106 Braunschweig, Germany; s.kipp@tu-bs.de[2]

ABSTRACT

The influence of different materials on the fouling tendency in saline calcium sulfate solution was investigated. The effects of the untreated material on the crystallization process have been studied experimentally in the micro- and macroscopic scale. The crystallization in the induction period was visualized with SEM and AFM to locate preferred nucleation spots and to visualize the crystal growth. The different materials are showing different crystal growth behavior (number and size of the crystals). These results are corresponding with the macroscopic fouling results with limited shear stress. Also different roughness values on stainless steel have been studied with respect to fouling tendency. The induction time can be extended with smoother surfaces due to the limitation of nucleation spots. With higher fluid velocities, the adhesion of the forming crystals on the heat transfer surface dominates the length of the induction time.

INTRODUCTION

Fouling is the undesirable forming deposit on technical used surfaces. Although the effects of e.g. crystallization fouling on costs and processes are well known, the first steps of crystallization on surfaces are still not completely understood. The process of surface crystallization is complex and starts with the nucleation and is followed by the crystal growth on this surface. But different surfaces (e.g. materials) have different fouling behaviors due to the different mechanical and energetic interactions on the interface surface/fluid. The decrease of efficiency due to fouling can be characterized by the fouling resistance R_f , which is defined by the equation

$$R_f = \frac{1}{k_f} - \frac{1}{k_0} \qquad (1)$$

where k_f is the overall heat transfer coefficient for the scaled and k_0 for the clean surface. In crystallization fouling the fouling curve can be subdivided into two major parts (see Fig. 1).

1. Induction period
2. Crystal growth

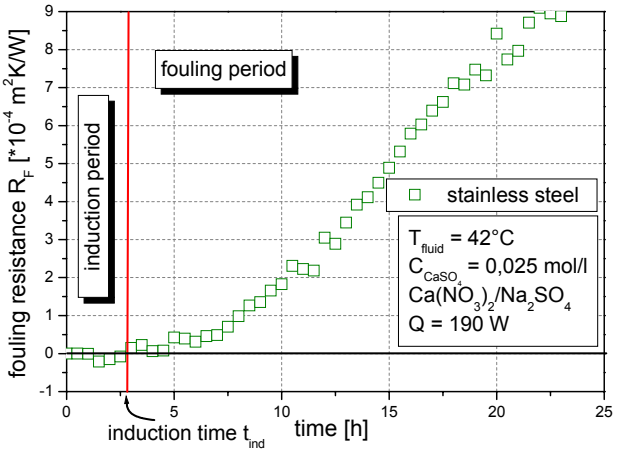

Fig. 1 Fouling resistance versus time for a crystallization fouling experiment with $CaSO_4$ on stainless steel

In the induction period, the nucleation of crystals on the surface begins and small crystals are formed. This additional layer is heterogeneous distributed on the surface and has no negative effect on heat transfer. In some cases, these additional formed roughness has a positive effect on the heat transfer due to induced wall near turbulence [Augustin 1994, Crittenden/Alderman 1988].

The fouling period is defined as the period, where the additional fouling layer has a negative influence on heat transfer. In this span of time the formed crystals are growing with an negligible influence of the interfaces surface/crystal and surface/liquid. The deposition in fouling period is mainly driven by the supersaturation of the liquid and the process conditions.

While the fouling period can be simulated [Brahim 2003] the influences and the mechanisms in the induction period are not completely known. To close this gap, this work is focused on the nucleation on different materials with a closer look on the induction period.

EXPERIMENTS

The effects on the length of the induction period are influenced by:

- Process condition
- Interface conditions

Table. 1 Influencing factors on the induction period of crystallization fouling

	Influences on crystallization fouling
Process conditions	Salt system
	Supersaturation and pH value
	Flow velocity (Reynolds number)
	Flow regime
	Additives
Interface conditions	Surface temperature (heat flow)
	Surface energetic (surface energy, zeta potential)
	Roughness and topography
	Amount of primarily nucleation spots
	Fluid interaction (aging of surface)

The aim of the project is the buildup of a database to calculate the induction time. This model must contain the main influencing factors (see Table 1) on the induction period and should be complemented with existing models of the crystal growth period (Augustin 1994, Brahim 2003). To reach this goal the influencing factors must be investigated separately with respect to crosswise impact of other factors (e.g. surface energy and roughness). In this paper the influence of the interface conditions except surface temperature and aging effects will be investigated.

Two fouling test units have been build up in order to validate the influences of different materials on induction time. Fig. 2 shows the batch fouling test unit. The simple design combined with defined process conditions allows a large number of fouling experiments. A detailed description of the batch test unit has been given by Augustin 2005 and Bohnet 2003.

The results of this fouling test units give an integral fouling resistance value and allows to compare the fouling resistance of different materials including induction and fouling period. All experiments are conducted at constant process conditions (25 mmol/l $CaSO_4$, Q=190 Watt, T_{Fluid}=42°C).

To take a closer look on the induction period a second fouling test unit was build-up which allows to follow crystallization step by step with an atomic force microscope (AFM).

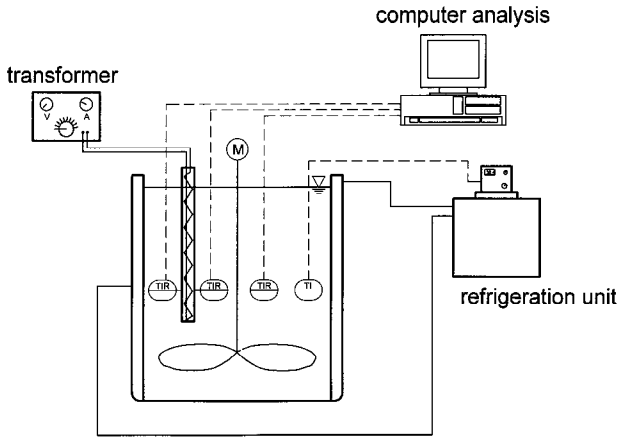

Fig. 2 Batch test unit for fouling experiments

As can be seen in Fig. 3 the general design is equal to the batch test unit to have maximum comparability. The salt solution is preheated to 42°C in the double shell tank (B1) and pumped with very low fluid velocity into the test section. The tested surface with the geometry of 20*80*2 mm^3 is fixed in the test section and heated by an electrical rod heater. On top of the test section an AFM is mounted with the possibility to scan the surface while crystallization starts. The visualization of the crystallization have been done outside of the fluid (ex situ). to get reproducible data based on the time dependent topographies. The in situ measurement is critical in form of measurement quality based on the influencing factors (thermal drift, tangential forces on the cantilever due the shear stress).

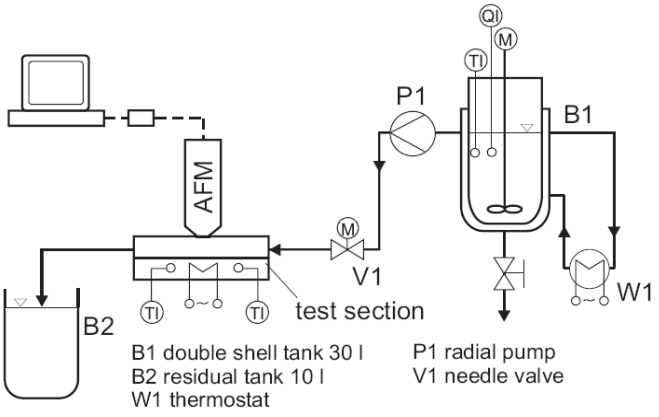

Fig. 3 Experimental setup for the visualization of the crystallization by AFM

With the AFM, the topography of the different materials or surfaces was characterized before the

crystallization process in order to get information of the cleaned surface.
The three dimensional roughness parameters used to describe the crystal growth are:

Ten point height of the surface S_z,

$$S_z = \frac{1}{5}\left(\sum_{i=1}^{5}|\eta_\pi| + \sum_{i=1}^{5}|\eta_{vi}|\right) \quad (2)$$

with,

$$\eta(x,y) = \left\{ I(x,y) - \left\{ \frac{1}{P}\sum_{j=1}^{N}\sum_{i=1}^{M} I(i,j)(i,j)\hat{I}A \right\} x=1\text{-}N; y=1\text{-}M; (x,y)\hat{I}A \right\}$$

the mean deviation of the surface S_a

$$S_a = \frac{1}{P}\sum_{j=1}^{N}\sum_{i=1}^{M}\left|\eta(i,j)\right| \quad (3)$$

and the developed interfacial area ratio S_{dr}

$$S_{dr} = \frac{\sum_{j=1}^{N-1}\sum_{i=1}^{M-1} A_{ij} - P'\Delta x\Delta y}{P'\Delta x\Delta y}\cdot 100\% \quad (4)$$

with

$$A_{ij} = \frac{1}{4}\left[\sqrt{\Delta y^2 + \left(\eta(i,j)-\eta(i,j+1)\right)^2} + \sqrt{\Delta y^2 + \left(\eta(i+1,j+1)-\eta(i+1,j)\right)^2}\right] \cdot \left[\sqrt{\Delta x^2 + \left(\eta(i,j)-\eta(i+1,j)\right)^2} + \sqrt{\Delta x^2 + \left(\eta(i,j+1)-\eta(i+1,j+1)\right)^2}\right]$$

which is defined as the increase of surface area related to a totally flat surface. For the ex situ measurements, the test plate were cleaned and dried. After the AFM measurement, the plates were mounted again in the test channel.

To get information about the macroscopic roughness, a roughness test unit (see Fig. 4) gives information about the mean roughness depth R_Z

$$R_Z = \frac{1}{5}\sum_{i=1}^{5} Z_i \quad (5)$$

while Z describes the absolute highest point in one section.

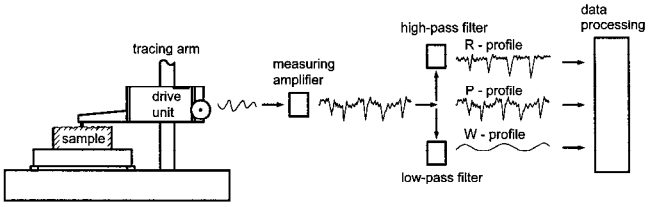

Fig. 4 Macroscopic roughness test unit

The energetic properties of the solid surface were measured with two different methods: the free surface energy and the zeta potential. The interfacial free surface energy was measured with an drop shape measurement equipment. The wetting of an droplet on a solid surface (see Fig. 5) leads to the Young equation :

$$\sigma_S = \gamma_{Sl} + \sigma_l \cdot \cos\theta \quad (6)$$

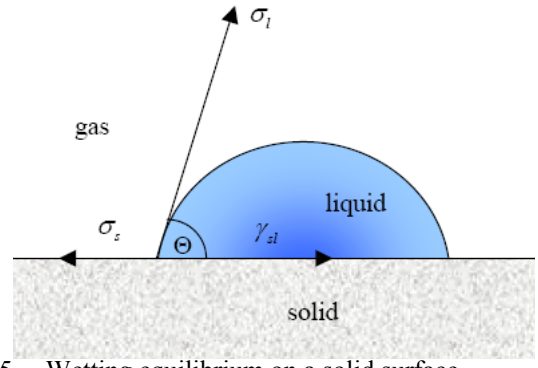

Fig. 5 Wetting equilibrium on a solid surface

To calculate the free surface energy, the contact angles of six different liquids were tested. The mean value of the contact angles for each liquid (see Tab. 2) are the calculation background for the Owen, Wendt, Rabel and Kaelble calculation, which divides the surface energy into polar and dispersive parts and is based on an linear regression [Owens 1969].

Table. 2: Physical properties of the used test liquids for surface energy measurements

Liquid	Dispersive part [mN/m]	Polar part [mN/m]
Water	21,80	51,00
Ethylene glycol	30,90	16,80
Formamide	39,00	19,00
1-Brom naphthalene	44,40	0,20
Glycerine	34,00	30,00
Dijodmethane	50,80	0,00

A second method to measure interfacial energies is the zeta potential. In ion containing liquids charged particles are surrounded by ions until the outside potential of the particle reaches zero. The ionic bond of the ions is reduced with larger distance to the charged particle, so two main regions can be described: The strongly bound inner region, so called

Stern layer and the weak bound outer layer, the so called diffusive layer, where the potential aspires to zero.

The most common method for zeta potential measurement is the electrophoretic mobility. When an electrical field is applied, the inhomogeneous outer region of the diffusive layer allows the particle to move to the opposite charged electrode. With this motion some parts of the diffusive layer do not move with the particle because of the force equilibrium between shear stress and attachment to the particle. This region is called the slipping plane, see Fig.6.

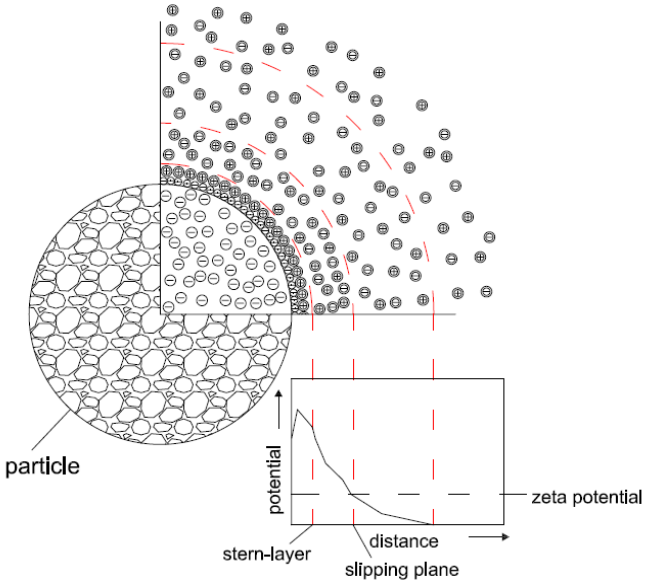

Fig. 6 Potential course of a charged particle

The velocity of this charged particle is measured with the laser doppler velocimetry (electrophoretic mobility) and is a function of the strength of the electrical field, the dielectric constant, the viscosity of the medium and the zeta potential.

The zeta potential is calculated with the Henry equation:

$$U_E = \frac{2 \cdot \varepsilon \cdot \zeta \cdot f(ka)}{3\eta} \qquad (7)$$

The factor f(ka) is calculated with the Smoluchowski approximation and is set to 1.5 which is common for larger particles (> 20 nm) [Müller 1996]. To detect the surface potential, zeta potential of particles of the surface as well as streaming potential of the surface is available. First comparative measurements of the particles of the surface and the surface itself have shown similar results.

VARIATION OF THE SURFACE ROUGHNESS

To detect the influence of surface roughness on the induction period of crystallization fouling, stainless steel plates were mechanically treated by different grinding papers (the name of the plate represents the grain size), paste or electropolished. The surface properties like roughness, surface energy and AFM measurements are done before the fouling measurements. The influence of different mechanically treatments on roughness and surface energy is shown in Fig. 7.

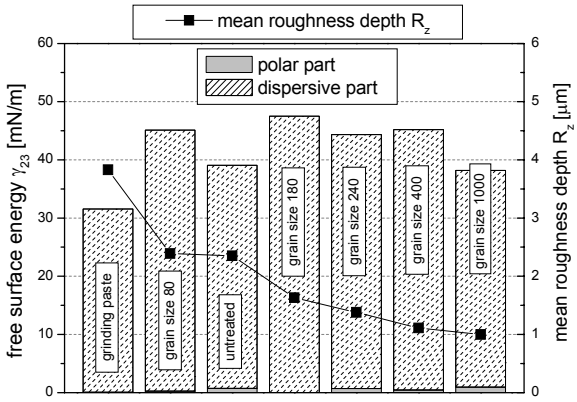

Fig. 7 Influence of different mechanically treatments of stainless steel on surface energy and mean roughness depth

The roughness as well as the surface energy are influenced by the mechanically treatment. The surface energy in form of residues of the grinding process inside the stainless steel surface and the surface topography through metal removal and deformation. Also the roughness itself has an influence on the measurement of the surface energy. This influence of roughness is well investigated by different authors [Busscher 1983, Palzer 2001, Wang 2004], but there is no link between industrial roughness parameter and influence on the surface energy till now.

In order to evaluate the influence of surface roughness on the induction period several different mechanically treated plates of stainless steel have been exposed to the liquid flow of an aqueous calcium sulfate solution. The concentration of $CaSO_4$ was 25 mmol/l prepared from $NaSO_4$ and Ca_2 $(NO3)_2$ and was controlled by titration.

Fig. 8 shows the result of the fouling experiments. The fouling resistance is related to the heat transfer area which is corrected by the S_{dr} factor from equation 4. It shows an dependence between the mean roughness depth and the induction time. A reduced mean roughness seems to enlarge the induction time. The roughness must be related to the number of possible nucleation spots, because the nucleation energy is reduced in valleys or peaks.

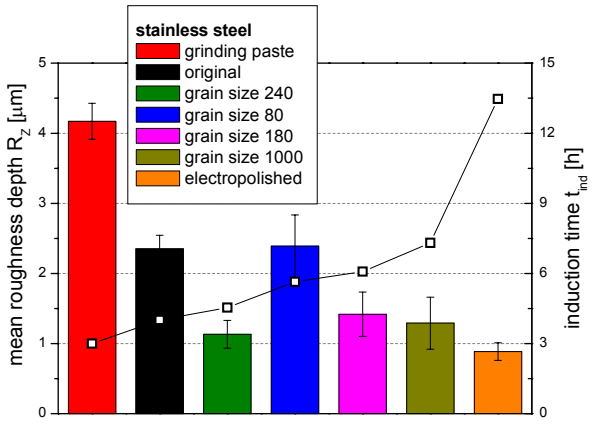

Fig. 8 Influence of the mean roughness depth of different mechanically treated stainless steel on induction time

Because of that, the combination of the enhancement of the surface by the real topography combined with the mean roughness depth is a first step, but it must be combined with another parameter describing the amount of specific roughness of the surface. This specific roughness must be related to the diameter of the first nucleation particles. The influence of the roughness on the heat transfer coefficient on the fluid side is excluded from the calculation and must be investigated separately. First results are showing a dependency between the heat transfer coefficient and the coverage of microstructures on the surface (see Fig. 9, Scholl 2006).

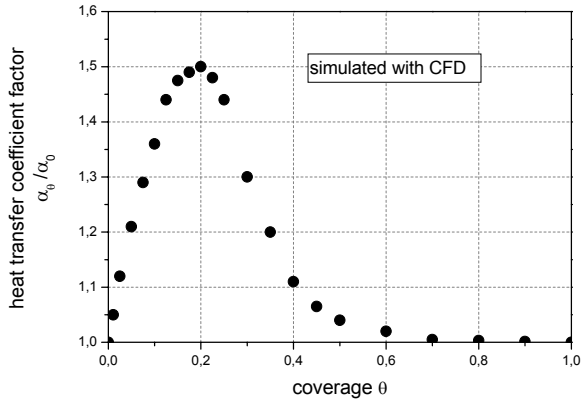

Fig. 9 Influence of the coverage of micro roughness on the simulated heat transfer coefficient (Scholl 2006)

The coverage Θ is the percentage allocation of pyramid-base shaped roughness elements on a totally flat heat transfer surface. The results of the simulation are showing an enhancement of the heat transfer coefficient up to 50 percent which can be related to the negative fouling resistance within the induction period. The next step in simulation must be the matching between simulated heat transfer enhancement and real growing crystals to get a better understanding of the negative fouling resistance and the induction time.

PREFFERED NUCLEATION SPOTS

Experiments have shown that crystallization on stainless steel normally starts at the grain boundaries of the surface. In this specific area, the activation energy for the heterogeneous crystallization is reduced. At higher flow velocities, these grain boundaries act like deadbands with reduced shear stress.

Different materials have different surface energies and different topographies (see Fig. 10). Also the chemical interaction with saline solution (corrosion) is different.

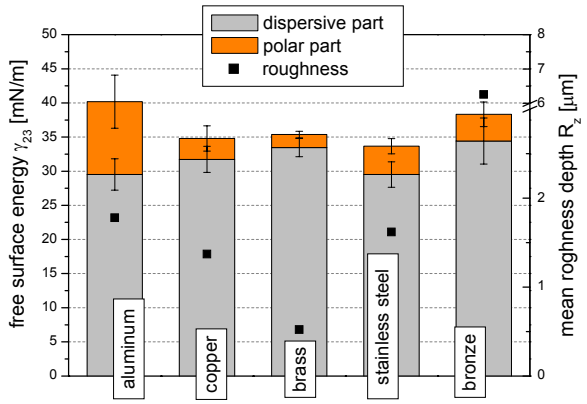

Fig. 10 Free surface energy calculated with Owens, Wendt, Rabel and Kaelble and mean roughness depth of different materials

These different surface characteristics lead to a different heterogeneous crystallization behavior of $CaSO_4$. The different topographies represented by the mean roughness depth should lead to different induction times (compare with Fig. 8) as well as different surface energies are related to different induction times [Augustin 06 and Förster 2000]. The different materials were tested in the batch test unit with very low fluid flow to exclude the influence of shear stress on the growth of the crystals. The low stirrer velocity is only liable for the decline of temperature and concentration gradient.

After short crystallization time (one hour, see Fig. 11, top) the plates are demounted and the crystallization is visualized with SEM images.

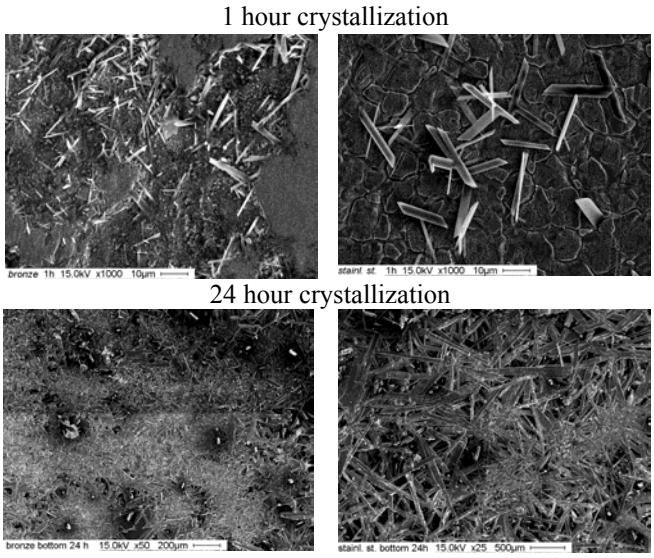

Fig. 11 SEM images of the crystallization process Left side: bronze (1h and 24h), right side: stainless steel

To combine these microscopic results with the macroscopic fouling experiments, SEM micrographs of the bottom side of the full grown saline layer were taken. These micrographs show the start of the heterogeneous crystallization on the heat transfer surface (see Fig 11). While $CaSO_4$ crystals on bronze are small with an high amount of nucleation spots after one hour crystallization, the crystals on stainless steel are larger and thicker. The amount of nucleation spots on stainless steel seems to be limited, but the few crystals are growing faster because of the nonexistence of inhibiting factors. The micrographs of the backside of the fouling layer is showing the same result: High amount of small crystals on bronze and fewer but larger crystals on stainless steel. To get a more detailed look on the fouling process in the induction period, AFM measurements were done during the induction period.

All AFM measurements are done ex-situ to reach a maximum resolution of the topography. Fig. 12 shows the crystal growth of $CaSO_4$ on stainless steel in the AFM test unit with an resolution of 100*100 μm^2. After a short time of 10 minutes, first crystals out of the grain boundaries have been formed. These crystals are growing by time while the measurement position on the stainless steel is fixed. All pictures contain information of the x, y and z coordinates for all image points. With these information's, the line scans of the AFM could be extract and evaluated at specific points were crystals are growing. The difference of these height profiles at different crystallization times gives an information about the crystal growth.

Fig. 13 shows profile scans at selected points on the tested materials with crystallization fouling in the AFM test

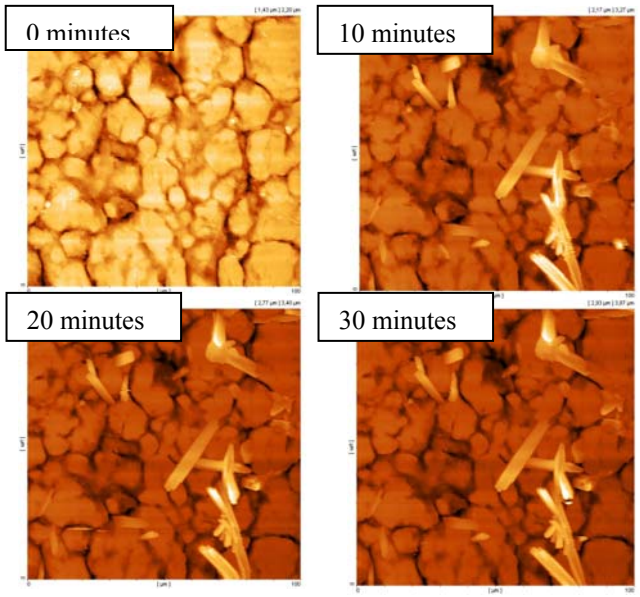

Fig. 12 AFM pictures of stainless steel while crystallization fouling takes place

unit. The results are showing a fast crystallization on aluminum, copper and bronze and a slower crystal growth on stainless steel and brass.

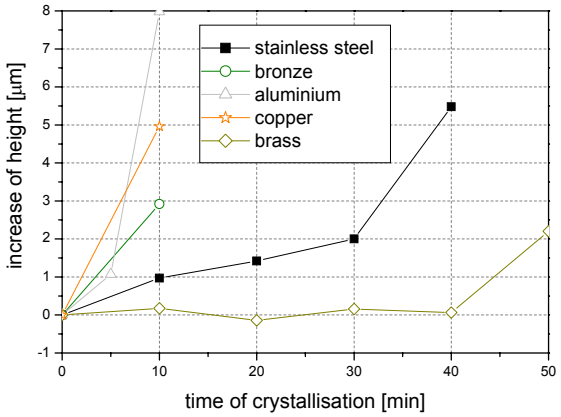

Fig. 13 Crystal growth on different surfaces (AFM)

These results must be correlated to the macroscopic roughness of the tested plates. While the roughness of bronze is very high and the crystal growth is medium, aluminum and copper are showing comparable roughness parameters to stainless steel, but faster crystal growth. Brass has a very smooth surface, which is reflected in the crystal growth value.

INFLUENCE OF DIFFERENT MATERIALS ON THE INDUCTION TIME

The macroscopic fouling resistance describes the time dependent crystallization process for industrial applications. All fouling experiments were carried out in a slowly stirred, temperature controlled vessel (see Fig. 2) and measuring solution temperature, pH as well as the surface temperature of the heating elements.

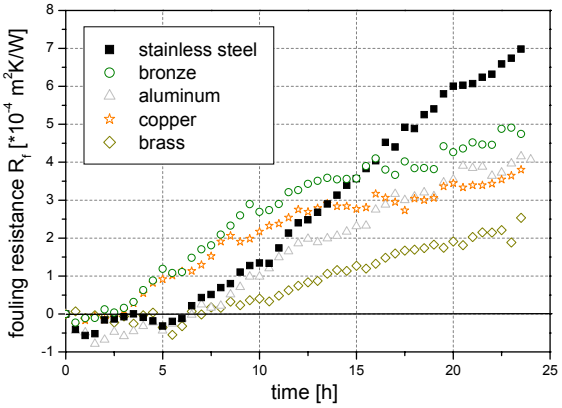

Fig. 14 Influence of different materials on the fouling tendency to $CaSO_4$

Fig. 14 shows the fouling curves for all tested materials. All curves are showing similar behavior. After a time period (induction time) where the fouling resistance is near or below zero the extensive surface crystallization takes place. While the crystal growth period is similar on every material, except of stainless steel, the induction time is different.

Because of inhomogeneous initial conditions, respective surface roughness and surface energy, no direct link between one surface characteristic is possible. But all materials are showing similar behavior in slow fluid flow conditions like the batch crystallization and the AFM measurements. The materials brass and stainless steel are showing a slow crystal growth which is comparable to a long induction time in the batch experiments. Copper and bronze showing nearly spontaneous crystal growth resulting in a short induction time. Only the crystallization behavior of aluminum differs between AFM and batch crystallization. Besides the different aging properties of the material, the interaction of the material with the saline fluid can be one statement. The interaction of the fluid with the material can be characterized by the zeta potential which is equivalent to the charge of the interface between material and fluid. This layer can influence the mass transport to the interface and so to the crystallization fouling (Park 2003).

The measurement of the zeta potential in high ionic strength (like 0,025 mol/l $CaSO_4$) is difficult because of the compression of the diffusive layer, so destilled water was used.

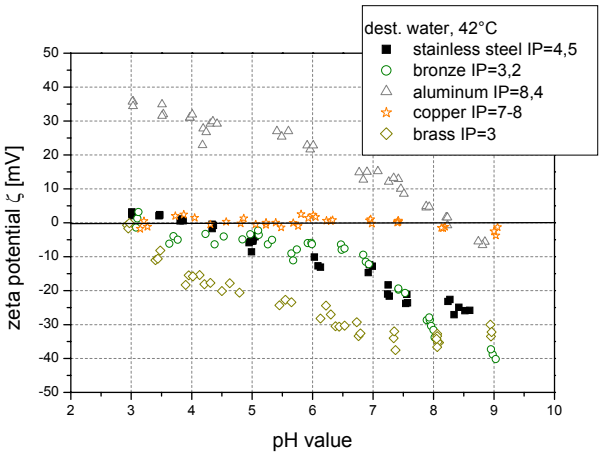

Fig. 15 Zeta potential versus pH value for different materials

Fig. 15 shows the difference between the tested materials and the pH dependent charge. In colloidal science the zeta potential defines areas of coalescence or agglomeration and stable particles or dispersion. When the charge of particles reaches zero the rejection forces are minimum. Only aluminum reaches low surface charge near the pH value of the fouling measurements (pH 7).

CONCLUSIONS AND PROSPECTS

The experimental results are displaying the change of the fouling tendency by different heat exchanger materials. Besides the surface roughness of the material, the energetic at the interface fluid/surface is a key factor in surface crystallization. With different visualization techniques like AFM and SEM, preferred crystallization spots and the crystal growth versus time are now accessible. The experiments with negligible influences of the fluid flow in AFM experiments and a batch test unit are showing similar results. The crystal growth on the materials copper and bronze is favored while the crystal growth on stainless steel and brass is much slower. These information's of the crystal growth must be related to the adhesion of Calcium sulfate on the different materials and the fluid velocity in real systems. The combination of a smooth surface and the right fluid shear stress related to the adhesion of the crystals on the heat transfer surface must lead to maximum induction time.

Future research will focus on the influence of different topographies on materials, the influence of pH on the crystallization compared to the zeta potential. When topography and energetic characteristics are known, tailored surfaces are the next step in preventing fouling.

ACKNOWLEDGEMENT

Financial support for this research project is granted by "Deutsche Forschungsgemeinschaft, DFG"

NOMENCLATURE

A	area, m^2
c	concentration, $mol\ l^{-1}$
f	Henry function
k	heat transfer coefficient, $W\ m^{-2}\ K^{-1}$
R_f	fouling resistance, $m^2\ K\ W^{-1}$
R_Z	mean roughness depth, m
S_a	mean deviation of the surface (3D), m
S_{dr}	interfacial area ration (3D), %
S_Z	ten point height (3D), m
T	temperature, °C
t	time, h
U_E	electrophoretic mobility $m^2\ V^{-1}\ s^{-1}$
w	flow velocity, $m\ s^{-1}$
Q	heat duty, W
γ_{ij}	interfacial free energy between two adjacent phases i and j, $N\ m^{-1}$
ε	dielectric constant, $A\ s\ V^{-1}\ m^{-1}$
η	viscosity, $kg\ m^{-1}\ s^{-1}$
θ	contact angle, degree
θ	coverage of the microstructures, %
ζ	zeta potential, V

Subscript

0	clean
d	deposition
f	fouling
fluid	fluid
ind	induction period
l	liquid

REFERENCES

Augustin, W., Zhang, J., Bialuch, I., Geddert, T. and Scholl, S., "*Modified DLC-Coatings for the Mitigation of Scaling on Heat Transfer Surfaces*" *Proc. "Enhanced, Compact and Ultra-Compact Heat Exchangers: Science, Engineering and Technology",* 2005, pp. 394-402

Augustin, W. and Bohnet, M., *"Modellierung des Foulingverhaltens von rauhen Wärme-tauscherrohren"* Chem. Ing. Tech., vol. 66, no. 10, 1994, pp. 1396-1399

Bohnet, M., Höfling, V. and Augustin, W., "*Crystallization Fouling Of The Aqueous Two-Component System CaSO4/CaCO3"* Proc. 2003 ECI Conference on Heat Exchanger Fouling and Cleaning: Fundamentals and Applications,

Brahim, F., *"Numerische Simulation des Kristallwachstums auf wärmeübertragenden Flächen (Fouling)"*, Dissertation, TU Braunschweig, Shaker, 2003

Busscher, H., Van Pelt, A., De Boer, P., De Jong, H. and Arends, J., *"The Effect of Surface Roughening of Polymers on measured Contact Angles of Liquids"* Colloids Surf. , no. 9, 1983, pp. 319-331

Crittenden, B. and Alderman, N., *"Negative Fouling Resistance: The Effect of Surface Roughness"* Chem. Eng. Sci. , vol. 43, no. 4, 1988, pp. 829-838

Förster, M. and Bohnet, M., 2000, *"Modification of Molecular Interactions at the Interface Crystal/Heat Transfer Surface to Minimize Heat Exchanger Fouling", Int. J. Th. Sci.*, Vol. 39, pp. 697-708

Müller, R. H., Nitzsche, R. and Paulke, B., *"Zetapotential und Partikelladung in der Laborpraxis. "* no. 37, 1996, pp. 7-254

Owens, D. and Wendt, R., *"Estimation of the free surface energy of polymers"* J. Appl. Polym. Sci., no. 13, 1969, pp. 1741-1747.

Palzer, S., Hiebl, C., Sommer, K. and Lechner, L., *"Einfluss der Rauhigkeit einer Feststoffoberfläche auf den Kontaktwinkel"* Chem. Ing. Tech., no. 73, 2001, pp. 1032-1038

Park, J., Lee, H., Choi, S., Geckeler, K. and Cho, J. M. S., *"Fouling mitigation of anione exchange membrane by zeta potential control"* J. Colloid Interface Sci., no. 259, 2003, pp. 293-300.

Scholl, S. and Augustin, W., *"Numerical Simulation of Micro Roughness Effects on Convective heat transfer"* Proc. 16th. European Symposium on Computer aided Process Engineering, Amsterdam, 2006, pp. 671-676

Wang, X., Peng, X., Lu, J., Liu, T. and Wang, B., *"Contact angle hysteresis on rough solid surfaces"* Heat transfer / Asian research, vol. 33, no. 4, 2004, pp. 201-210